Alkali-halogen metasomatism of the CM carbonaceous chondrites

The Meteoritical Society

Meteoritics & Planetary Science 1–12 (2019)
doi: 10.1111/maps.13405

Alkali-halogen metasomatism of the CM carbonaceous chondrites

M. R. LEE [1,*], B. E. COHEN [1,2], and A. J. KING [3,4]

[1]School of Geographical and Earth Sciences, University of Glasgow, Gregory Building, Lilybank Gardens, Glasgow G12 8QQ, UK
[2]Present address: School of GeoSciences, University of Edinburgh, Grant Institute, Edinburgh EH9 3FE, UK
[3]Department of Earth Science, Natural History Museum (London), Cromwell Rd, London SW7 5BD, UK
[4]Present address: School of Physical Sciences, The Open University, Walton Hall, Milton Keynes MK7 6AA, UK
[*]Corresponding author. E-mail: martin.lee@glasgow.ac.uk

(Received 29 October 2018; revision accepted 26 September 2019)

Abstract–Meteorite Hills (MET) 01075 is unique among the CM carbonaceous chondrites in containing the feldspathoid mineral sodalite, and hence it may provide valuable evidence for a nebular or parent body process that has not been previously recorded by this meteorite group. MET 01075 is composed of aqueously altered chondrules and calcium- and aluminum-rich inclusions (CAIs) in a matrix that is predominantly made of serpentine- and tochilinite-rich particles. The chondrules have been impact flattened and define a foliation petrofabric. Sodalite occurs in a 0.6 mm size CAI that also contains spinel, perovskite, and diopside together with Fe-rich phyllosilicate and calcite. By analogy with feldspathoid-bearing CAIs in the CV and CO carbonaceous chondrites, the sodalite is interpreted to have formed by replacement of melilite or anorthite during alkali-halogen metasomatism in a parent body environment. While it is possible that the CAI was metasomatized in a precursor parent body, then excavated and incorporated into the MET 01075 parent body, in situ metasomatism is the favored model. The brief episode of relatively high temperature water–rock interaction was driven by radiogenic or impact heating, and most of the evidence for metasomatism was erased by subsequent lower temperature aqueous alteration. MET 01075 is very unusual in sampling a CM parent body region that underwent early alkali-halogen metasomatism and has retained one of its products.

INTRODUCTION

All of the CM carbonaceous chondrites have undergone extensive parent body aqueous alteration, which has been dated to 4563.4 +0.4/–0.5 Ma using the carbonate ^{53}Mn-^{53}Cr system (Fujiya et al. 2012). The alteration products are dominated by serpentine-group phyllosilicates, which comprise 56–88 vol% of bulk CMs (Howard et al. 2015; King et al. 2017) and are intergrown with carbonates, (hydr)oxides, sulfates, and sulfides (McSween 1979a, 1979b; Bunch and Chang 1980; Barber 1981; Lee 1993; Lee et al. 2012). The water that was responsible for this alteration came from accreted ices that were melted by heat generated from the decay of short-lived isotopes (principally ^{26}Al; Grimm and McSween 1989), and possibly also from impacts (Rubin 2012). Ambient temperatures during aqueous alteration have been estimated by a variety of methods including thermodynamic modeling (1–25 °C, Zolensky et al. 1989), oxygen isotope fractionation between alteration products (80 °C, Baker et al. 2002), carbonate oxygen isotopic compositions (0–130 °C, Alexander et al. 2015; 113 ± 54 °C, Verdier-Paoletti et al. 2017), and clumped isotope thermometry (20–71 °C, Guo and Eiler 2007). A subset of the CMs have evidence for later (i.e., posthydration) heating to temperatures sufficient to dehydroxylate the phyllosilicates (Akai 1988, 1992), and impacts are again a potential heat source (e.g., Nakamura 2006).

Here, we describe sodalite in the CM carbonaceous chondrite Meteorite Hills (MET) 01075. This mineral has not been previously found in a CM, but feldspathoids occur in CV and CO carbonaceous chondrites where they are interpreted to have formed during relatively high temperature (>~100 °C) Fe-alkali-halogen metasomatism within the parent body (e.g., Krot et al. 1995; Brearley

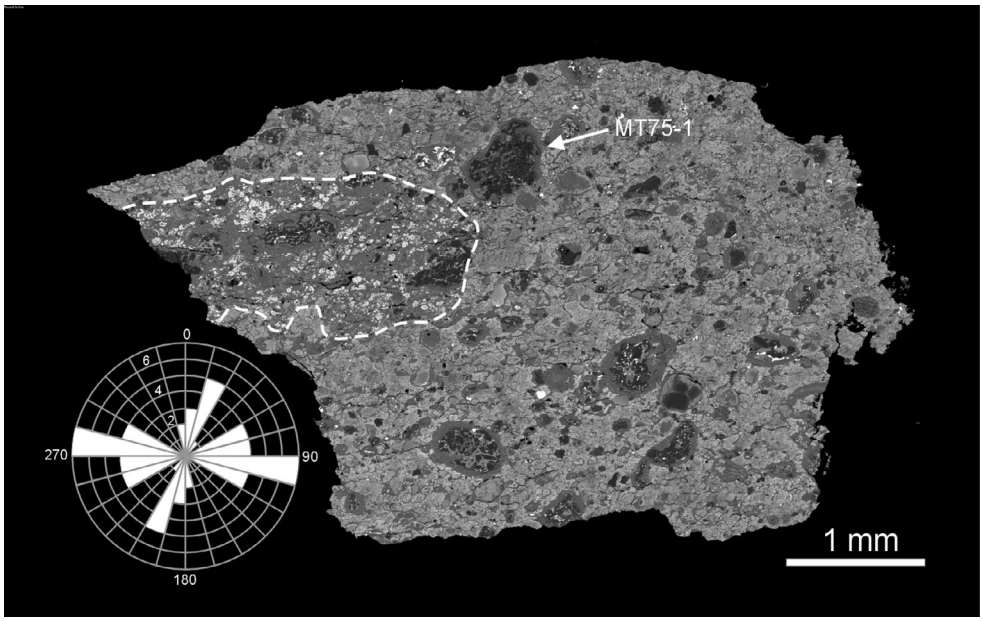

Fig. 1. BSE image of the MET 01075 polished block, which is dominated by the primary accretionary rock lithology. Its chondrules and chondrule fragments have fine-grained rims that stand out from TCI particles by virtue of their lower mean atomic number. The CAI MT75-1 is indicated. A second lithology, probably a clast, is outlined with a dashed white line. The inset rose diagram shows the orientations of the long axes of 30 chondrules and chondrule fragments in the primary accretionary rock lithology.

and Krot 2013). A finding that MET 01075 sodalite has formed in the same way would raise important questions, for example, (1) did this meteorite's parent body evolve differently to that of other CMs? or (2) is MET 01075 unique in preserving evidence for relatively high temperature water–rock interaction that was widespread within the CM parent body(ies)? In order to address these and other questions, we first describe MET 01075 with a focus on evidence for its parent body history, then give an account of the petrographic context and properties of the sodalite, and finally evaluate and discuss potential origins for the sodalite with reference to previous work on feldspathoids in other groups of carbonaceous chondrites.

MATERIALS AND METHODS

MET 01075 has a recovered mass of 29.94 g, a weathering grade of B, and is paired with MET 01071, MET 01072, and MET 01078 (Russell et al. 2003). We undertook scanning electron microscopy (SEM), electron probe microanalysis (EPMA), and transmission electron microscopy (TEM) on a single resin-mounted polished block, itself made from a 0.338 g subsample loaned by ANSMET (MET 01075,8; Fig. 1). A 89.8 mg subsample of MET 01075,8 was analyzed for its mineralogy by X-ray diffraction (XRD).

After coating with 5 nm of carbon, the polished block was studied at the University of Glasgow using a Zeiss Sigma SEM. This instrument is equipped with Oxford Instruments X-Max silicon-drift X-ray detector that is operated through Oxford Instruments INCA and AZtec software. The SEM was operated at 20 kV/2 nA and at high vacuum, and was used to obtain backscattered electron (BSE) images and X-ray point analyses and maps. The apparent size of chondrules and chondrule fragments was measured from BSE images, and calculated as (long axis + short axis)/2, where the short axis is the size measured midway along the long axis. X-ray maps were acquired at a resolution of 1024 × 788 pixels. For quantitative chemical analyses of the matrix and fine-grained rims, X-ray spectra were acquired with a count time of 60 s and using a ~275 to 400 μm^2 raster. The spectra were quantified using INCA software and with calibrations from the following standards: Na (jadeite), Mg (periclase), Al (corundum), Si (diopside), S (pyrite), K (orthoclase), Ca (wollastonite), Ti (rutile), Cr (chromite), Mn (rhodonite), Fe (garnet), Ni (Ni-metal). Typical detection limits are as follows (wt%): Na_2O (0.10), MgO (0.07), Al_2O_3 (0.11), SiO_2 (0.11), S (0.08), K_2O (0.09), CaO (0.12), TiO_2 (0.10), Cr_2O_3 (0.28), MnO (0.22), FeO (0.23), Ni (0.26). Quantitative chemical analyses of spinel, perovskite, diopside, and sodalite were obtained by EPMA using a CAMECA SX100 electron probe at the University of Edinburgh. The following mineral standards were used: Al, Na (jadeite), Mg (spinel), Ca, Si (wollastonite), Cl (halite), K (orthoclase),

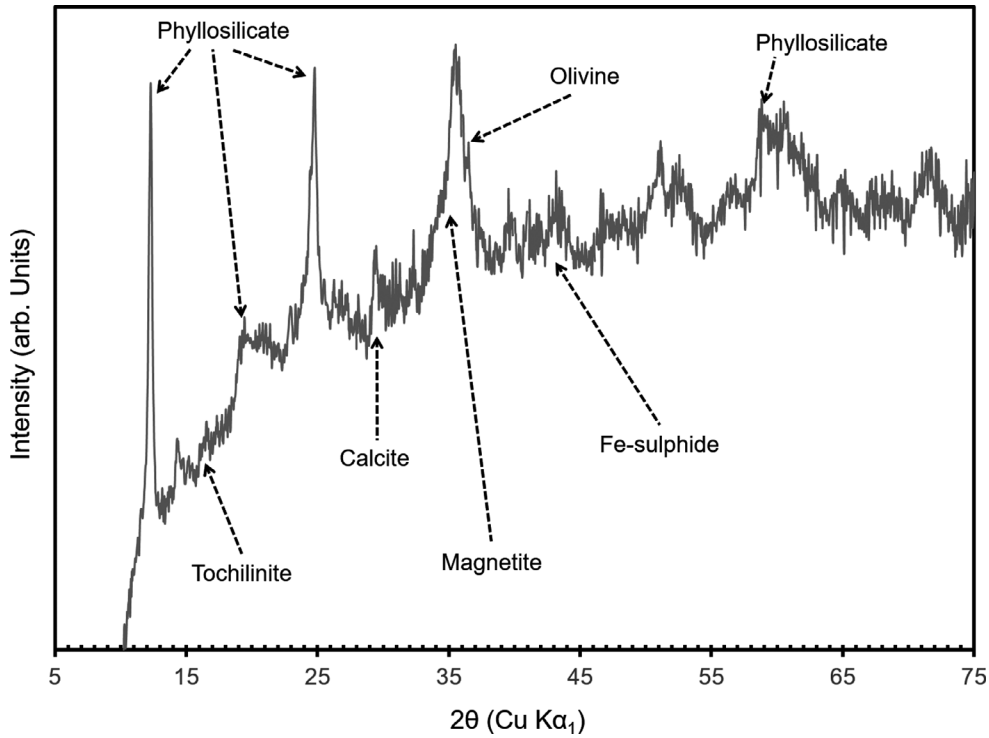

Fig. 2. XRD pattern of MET 01075 with the main peaks labeled.

Ti (rutile), Cr (Cr-metal), Fe (fayalite), Mn (Mn-metal). The 15 kV beam used a spot size of 3 μm for sodalite and 1 μm for diopside, spinel, and perovskite. Typical detection limits are as follows (wt%): Na_2O (0.01), MgO (0.05), Al_2O_3 (0.09), SiO_2 (0.06), Cl (0.11), K_2O (0.01), CaO (0.04), TiO_2 (0.10), Cr_2O_3 (0.02), MnO (0.03), FeO (0.04).

Electron-transparent samples for TEM at the University of Glasgow were extracted from the polished block using an FEI DualBeam focused ion beam instrument operated using 30 kV Ga^+ ions. The milling process followed the procedure of Lee et al. (2003) with samples being lifted out using an in situ micromanipulator and welded to the tines of a Cu holder using ion beam deposited platinum. TEM work used an FEI Tecnai T20 operated at 200 kV, with images captured with a Gatan off-axis TV-rate camera, and selected area electron diffraction patterns acquired using an SIS Megaview III CCD camera.

The XRD work was undertaken at the Natural History Museum (London) using an INEL X-ray diffractometer with a curved 120° position-sensitive detector in a static geometry relative to the X-ray beam and sample. The subsample of MET 01075 was ground to a powder and then packed into an aluminum sample well. Cu $K\alpha_1$ radiation was selected and the size of the beam on the sample was restricted to 0.24 mm × 2 mm using post-monochromator slits. XRD patterns were collected from the sample for 16 h, and from pure standards of minerals present in the meteorite for 30 min. Phase quantification used an XRD pattern profile-stripping method, with modal abundances limited to phases present at ≥1 vol% and with uncertainties of <5% (e.g., Cressey and Schofield 1996; King et al. 2015).

RESULTS

Mineralogy of MET 01075

The phases identified in MET 01075 by XRD are as follows: phyllosilicates (Fe-bearing serpentines), olivine, enstatite, magnetite, Fe-sulfides (pyrrhotite and pentlandite), tochilinite, calcite, and gypsum (Fig. 2; Table 1). The XRD pattern and mineral assemblage of MET 01075 are typical for CM carbonaceous chondrites (e.g., Howard et al. 2015). The abundance of tochilinite was not quantified because we lack a pure standard for the profile-stripping. However, as tochilinite in the CMs is commonly intergrown with Fe-cronstedtite, it is accounted for when subtracting this phase, as indicated by a final residual of zero counts after the profile-stripping. The phyllosilicate fraction (PSF = phyllosilicate abundance/[phyllosilicate + silicate abundance]) for MET 01075 is 0.87, which corresponds to a petrologic type of 1.3 on the scale of Howard et al. (2015; in their scale type 1.0 is a completely hydrous with >95 vol% phyllosilicate and type 3.0 is completely anhydrous with <5 vol% phyllosilicate).

Table 1. Modal mineral abundances in MET 01075 measured by XRD.

	Vol%
Olivine	9.7
Enstatite	2.8
Magnetite	1.4
Sulfides	2.7
Calcite	0.6
Gypsum	0.2
Fe-cronstedtite	18.7
Mg-serpentine	63.9
Total phyllosilicate	82.6
Phyllosilicate fraction	0.87
Petrologic type*	1.3

*Relative to the classification scheme of Howard et al. (2015).

Petrography and Chemical Composition

The polished block contains two lithologies (Fig. 1). The constituents of the dominant lithology, as determined by SEM point counting (n = 403 points), are as follows: 77 vol% fine-grained matrix, 12 vol% chondrules/chondrule fragments, 6 vol% fine-grained rims, 2 vol% calcium- and aluminum-rich inclusions (CAIs), and 2 vol% calcite. The fine-grained matrix is composed almost exclusively of ~30 to 70 μm size subrounded particles (Figs. 1 and 3A) that are made of fibers rich in O, Mg, Si, S, and Fe. This composition suggests that the fibers comprise serpentine (probably cronstedtite) intergrown with tochilinite, which is consistent with high-resolution TEM images (Fig. 3B) and analytical totals of ~89 wt% indicating the presence of unanalyzed H_2O/OH (Table 2). The particles are lined by selvages of a lower Z material that are up to ~10 μm in thickness (Fig. 3A). Metzler et al. (1992) described petrographically and compositionally similar particles as "PCP objects," and coined the term "primary accretionary rock" for lithologies that are dominated by them. Hereafter, the PCP objects are referred to as tochilinite–cronstedtite intergrowth (TCI) particles. Chondrules, chondrule fragments, and CAIs are enclosed by fine-grained rims that lack tochilinite fibers and so stand out in BSE images by virtue of their lower Z than the matrix (Fig. 3C). These rims are also compositionally different to the fine-grained matrix, principally with respect to Mg, Si, S, and Fe, but their low totals (~83 wt%) again indicate that phyllosilicates are abundant (Table 2). Chondrules and chondrule fragments contain phenocrysts of olivine and pyroxene together with Fe-rich phyllosilicates (Fig. 3C). They range in apparent diameter from 64 to 498 μm (average 156 ± 92 μm, ± 1SD n = 30). Many of them are flattened, with aspect ratios of 1.19–5.46 (average 2.03 ± 0.85 ± 1SD , n = 30), thus giving the primary accretionary rock a foliation petrofabric (Fig. 1). Those objects whose long axes have an orientation of 60/240°–105/285° in the rose diagram (Fig. 1) are the most highly flattened. Calcite grains are evenly distributed throughout the primary accretionary rock and are up to 0.2 mm in size.

The subordinate lithology is elongate, 2 mm on its long axis, and is likely to be a clast. Its fine-grained matrix also contains TCI particles (Fig. 3D), which are less abundant than in the primary accretionary rock and have higher concentrations of S and Fe relative to Mg and Si, thus suggesting that tochilinite is their main constituent. Its two chondrules have apparent sizes of 442 and 345 μm, and both are flattened (aspect ratios of 2.04 and 3.89, respectively). The orientation of flattening is similar to the primary accretionary rock (Fig. 1). Calcite grains in the clast are smaller and less abundant than in the primary accretionary rock lithology.

The Sodalite-Bearing CAI

Sodalite occurs in a 0.6 mm diameter CAI within the primary accretionary rock lithology, hereafter called MT75-1 (Figs. 1 and 4A). MT75-1 is composed of ~4 μm size crystals of spinel that have abundant ~2 μm size inclusions of perovskite (Table 3; Fig. 4). Between the spinel crystals are grains of calcite and sodalite, and patches of fine-grained phyllosilicate (Table 3; Fig. 4). The sodalite grains are ~20 to 40 μm in size, and the euhedral terminations of some are outlined by phyllosilicates (Fig. 5). MT75-1 has a narrow (~7 μm) rim that is composed of ~2 μm size diopside crystals with a considerable compositional range (Table 3). The CAI is enclosed by a fine-grained rim that thickens into embayments and thins around protuberances to give it a rounded outline (Fig. 4A).

DISCUSSION

In order to understand the origin of sodalite in the CAI MT75-1, we first discuss the history of its host meteorite with a focus on the three most obvious effects of parent body processing, namely aqueous alteration, compaction, and incorporation of the clast. From an understanding of the evolution of MET 01075, we outline and evaluate pre- and post-accretionary scenarios for the origin of the sodalite. We conclude by considering the implications of our findings for models of CM parent body evolution.

Parent Body Processing

The presence of phyllosilicates in chondrules/chondrule fragments and the CAI, in addition to fine-

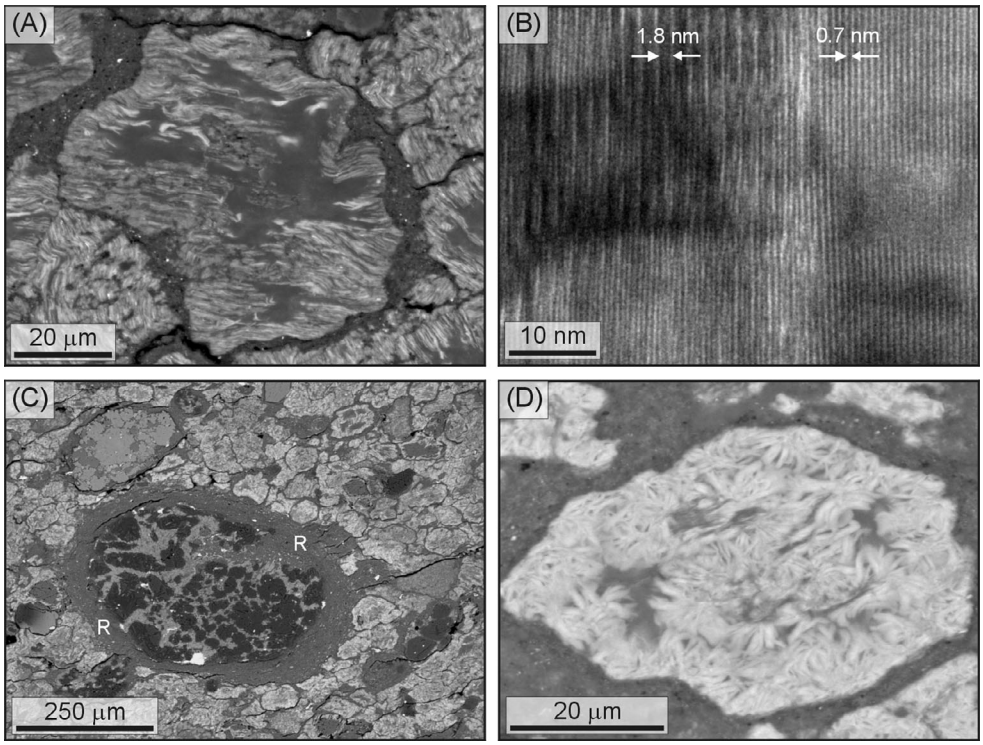

Fig. 3. Images of MET 01075. A) BSE image of a TCI particle that is composed of wavy fibers of tochilinite and serpentine. The particle is lined by a selvage of low Z phyllosilicate. B) High-resolution TEM image of the interior of a TCI particle. Tochilinite intergrown with serpentine is on the left-hand side (~1.8 nm lattice fringe spacing) and serpentine on the right (~0.7 nm lattice fringe spacing). C) BSE image of an area of primary accretionary rock that contains a rimmed chondrule. The primary accretionary rock is composed mainly of TCI particles, which have a significantly higher Z than the chondrule's fine-grained rim (R). D) BSE image of a TCI particle within the clast. Its constituent fibers have a lower aspect ratio and higher mean atomic number than the TCI particle in (A).

grained rims and the matrix, demonstrates that MET 01075 has undergone considerable aqueous alteration. XRD results show that it has a petrologic type of 1.3 (Table 1), which is equivalent to a CM2.2 on the scale of Rubin et al. (2007; whereby a subtype of CM2.0 is completely altered and C3.0 is completely unaltered). This classification is consistent with Lindgren et al. (2015), who estimated that its pair, MET 01072, has a petrologic subtype of CM2.3. From the concentration of H in water/OH, Alexander et al. (2013) assigned both MET 01072 and MET 01075 to a petrologic type of 1.5 (in their classification type of 3.0 is completely unaltered and type 1.0 is fully hydrated). However, Alexander et al. (2012, 2013) described MET 01075 and MET 01072 as "Heated ?" They suggested that both meteorites may have lost H accompanying partial dehydroxylation during post-hydration heating because their bulk H contents are ~0.2 to 0.3 wt% lower than unheated CMs with a similar deuterium/hydrogen ratio (i.e., δD).

The possibility that MET 01075 was heated after aqueous alteration is very important for evaluating its

Table 2. Chemical composition (wt%) of MET 01075 matrix and fine-grained rims.

	Matrix	Fine-grained rims
n	20	19
SiO_2	28.0 ± 2.2	34.2 ± 0.9
TiO_2	0.09 ± 0.08	0.05 ± 0.07
Al_2O_3	2.5 ± 0.3	2.3 ± 0.1
Cr_2O_3	0.21 ± 0.18	0.72 ± 0.12
FeO	34.5 ± 2.7	18.4 ± 0.7
MnO	0.14 ± 0.13	0.19 ± 0.14
NiO	1.4 ± 0.4	2.6 ± 0.3
MgO	17.0 ± 1.2	20.9 ± 0.7
CaO	0.07 ± 0.09	0.63 ± 0.46
Na_2O	0.28 ± 0.09	0.49 ± 0.10
K_2O	d.l.	d.l.
S	4.4 ± 1.3	2.3 ± 0.2
Total	88.6	82.9

d.l. below detection limits.
± 1SD.
The raster sizes for analyses of the matrix and fine-grained rims were ~400 and ~275 μm^2, respectively.

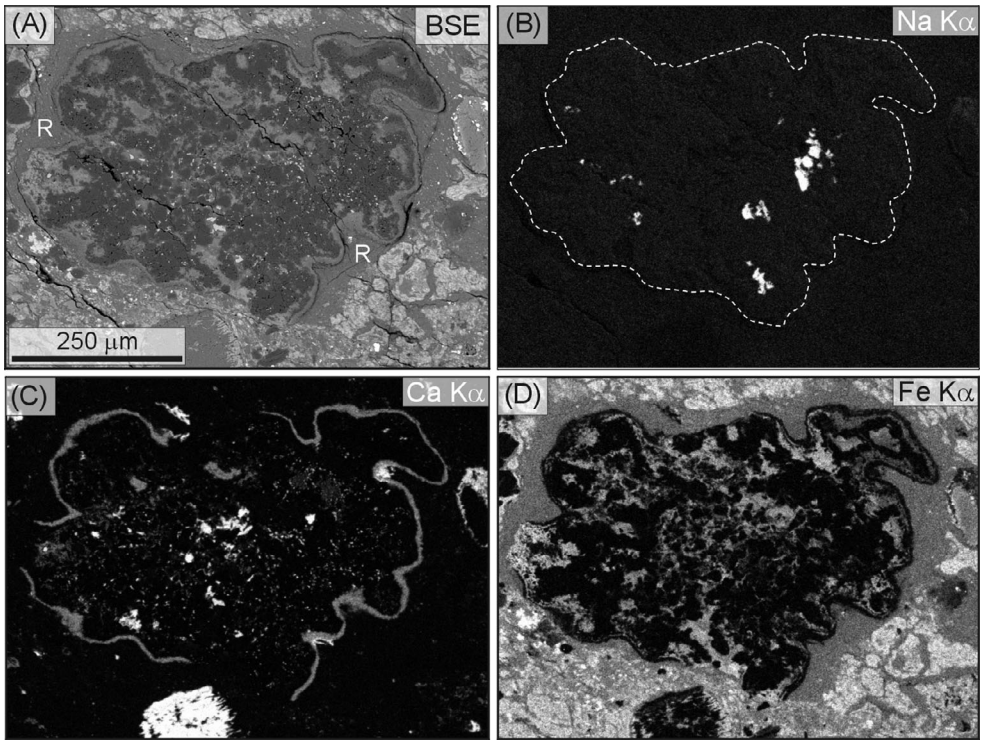

Fig. 4. The CAI MT75-1. A) BSE image of the CAI and its fine-grained rim (R). Spinel (mid-gray) is the most abundant constituent of the CAI. B) Sodium X-ray map highlighting grains of sodalite (white). The CAI is outlined by the dashed white line. C) Calcium X-ray map showing the location of calcite (white) within the CAI and the primary accretionary rock. This map also highlights abundant small perovskite grains (mid-gray) and the narrow diopside rim of the CAI (light gray). Note that the diopside rim is absent at three prominences, one at the base of the CAI, one at the top, and the third on its left hand side. D) Iron X-ray map. The principal Fe-rich minerals within the CAI are phyllosilicates (light gray).

Table 3. Chemical composition (wt%) of minerals within the MT75-1 determined by EPMA.

	Spinel	Perovskite	Diopside	Al-Ti Diopside	Sodalite
n	25	7	1	1	6
SiO_2	0.05 ± 0.07	0.33 ± 0.36	46.7	34.4	37.0 ± 0.5
TiO_2	0.25 ± 0.03	56.2 ± 0.6	2.7	9.2	n.a.
Al_2O_3	69.9 ± 0.6	0.84 ± 0.32	12.0	19.0	31.4 ± 0.8
Cr_2O_3	0.10 ± 0.05*	d.l.	0.11	0.16	n.a.
FeO	0.33 ± 0.07	0.59 ± 0.12	1.0	4.2	0.35 ± 0.25
MnO	d.l.	d.l.	0.03	0.05	d.l.
MgO	28.4 ± 0.3	0.19 ± 0.31	12.7	10.2	0.60 ± 0.76
CaO	0.03 ± 0.05	39.6 ± 0.3	24.4	21.4	0.05 ± 0.02
Na_2O	d.l.	d.l.	0.11	0.14	24.9 ± 0.6
K_2O	n.a.	n.a.	n.a.	n.a.	0.03 ± 0.01
Cl	n.a.	n.a.	n.a.	n.a.	6.8 ± 0.4
O=Cl	–	–	–	–	1.5 ± 0.09
Total	99.1	97.7	99.7	98.8	99.6
En	–	–	41.1	36.4	–
Fs	–	–	1.9	8.4	–
Wo	–	–	57.0	55.2	–

n.a. = not analyzed.
d.l. = below detection limits.
±1SD.
The two diopside analyses have been chosen to illustrate the compositional range.
*Only 20 of the analyses included Cr.

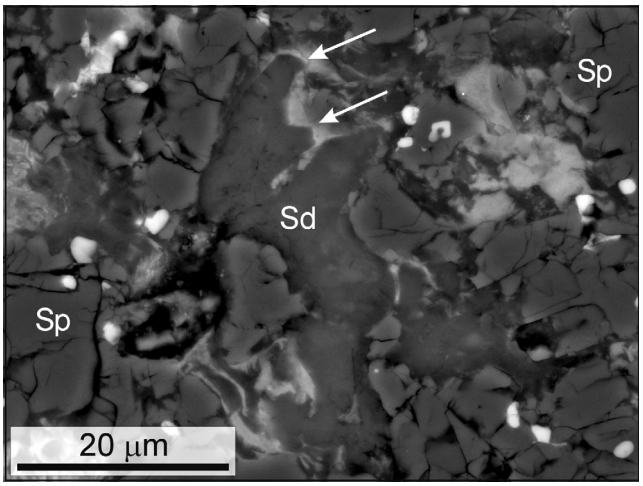

Fig. 5. BSE image of the patch of sodalite (Sd) close to the base of MT75-1 (Fig. 4B). Sodalite is surrounded by spinel (Sp), perovskite (small white crystals), and patches of phyllosilicate (light gray). Phyllosilicates outline the euhedral terminations of several sodalite crystals (arrowed).

parent body history. The intensity of posthydration heating that MET 01075 could have experienced is constrained by tochilinite and serpentine, which give sharp peaks in XRD patterns comparable to many other CMs, thus demonstrating that their crystal structures are intact. Estimates of the temperature at which tochilinite breaks down range from 120 °C (Zolensky et al. 1997) to 300 °C (Tonui et al. 2014). The thermal alteration of CM serpentine was investigated by Akai (1992), who described a series of transitional structures that develop between its initial breakdown at ~300 °C and crystallization of olivine/enstatite at ~750 °C (the transition temperatures have a minor time dependence). Another way to test the suggestion that MET 01075 had been heated is to determine whether the concentration of H predicted from the amount of phyllosilicate that it contains equals its H content as measured by Alexander et al. (2012), and similar calculations were undertaken by Alexander et al. (2013). If the phyllosilicates had lost some of their H from thermal dehydroxylation, the measured H content of MET 01075 should be lower than the amount of H that it is predicted to contain from its abundance of phyllosilicate. XRD shows that MET 01075 contains Mg-serpentine (63.9 vol%) and cronstedtite (18.7 vol%), which account for 1.107 wt% H (stoichiometric Mg-serpentine and cronstedtite have 1.44 and 1.00 wt% H, respectively). The meteorite also contains organic matter, which adds 0.087 wt% H, making a total of 1.195 wt% H (MET 0.075 has 1.59 wt% C, and the organic matter is assumed to have a H/C ratio of 0.055; Alexander et al. 2013). The value of 1.195 wt% H predicted from the abundance of phyllosilicate and organic matter is 0.08 wt% greater than the 1.117 wt% H measured by Alexander et al. (2012). While this result could argue for mild dehydroxylation of MET 01075 (i.e., the meteorite contains slightly less H than expected given its volume of phyllosilicate and organic matter), the small discrepancy in H content could also reflect differences in modal mineralogy between the subsamples of MET 01075 studied here and by Alexander et al. (2012, 2013). This difference in modal mineralogy between samples of the same meteorite could be due to the presence of clasts, which are commonplace in the CMs (e.g., Bischoff et al. 2006) and occur in MET 01075 (i.e., Fig. 1). These calculations therefore support inferences from the crystallinity of tochilinite and serpentine that MET 01075 was not significantly heated after aqueous alteration.

The other two obvious effects of parent body processing are compaction and incorporation of the clast. Both MET 01075 and MET 01072 have a compactional petrofabric that is defined by flattened chondrules/chondrule fragments, and the degree of flattening is similar between samples of the two meteorites (average chondrule aspect ratios of 2.03 and 1.68 for MET 01075 and 01072, respectively; Lindgren et al. 2015). These petrofabrics are fairly common within the CMs, where they are interpreted as being impact generated because lithostatic pressures would have been insufficient to generate such a degree of compaction (Rubin 2012; Hanna et al. 2015; Lindgren et al. 2015). Although most CMs belong to shock stage S1 (Scott et al. 1992) and so did not experience high impact pressures, the petrofabrics could have formed from one or more lower intensity collisions (Lindgren et al. 2015). There are, however, no clear petrographic indicators of whether impact compaction took place before, during, or after aqueous alteration. The clast is interpreted to have been juxtaposed with the primary accretionary rock lithology after both had been aqueously altered as they differ significantly in mineralogy (e.g., abundance and grain size of calcite). These two lithologies could have been mixed at the same time as the petrofabric-forming impact or the clast could have been incorporated in a later event.

Pre-Accretionary Formation of Sodalite

The presence of a sodalite-bearing CAI in an otherwise feldspathoid-free meteorite could be explained by the sodalite having formed before MT75-1 was incorporated into the MET 01075 parent body. Two possible pre-accretionary environments are the solar nebula and a precursor parent body. Secondary minerals including feldspathoids in CAIs from the CV3 meteorites have been interpreted to have formed by alteration in the solar nebula (e.g., Palme and Wark 1988; Ikeda and Kimura 1995, 1996), although petrography, mineralogical,

chemical, and isotopic evidence now supports an origin by Fe-alkali-halogen metasomatism in the CV parent body (e.g., Krot et al. 1995, 1998a, 1998b). The discussions below therefore assume a parent body origin for MET 01075 sodalite by analogy with the CVs, although we have no direct evidence regarding a nebular origin.

The other pre-accretionary scenario for MET 01075 sodalite is metasomatism of MT75-1 in a CV-like precursor parent body. However, as the CAI is largely intact, and occurs as a discrete rimmed object within the primary accretionary rock (i.e., is not part of a clast), the scenario of metasomatism in a precursor parent body followed by impact excavation and reaccretion is unlikely. Another argument against the derivation of MT75-1 from a CV-like parent body is that its spinel-perovskite-diopside mineralogy is typical of CAIs in other CM meteorites (Greenwood et al. 1994) but dissimilar to CAIs in the CVs. We therefore argue that the sodalite formed after MT75-1 had been accreted into the MET 01075 parent body.

Parent Body Alkali-Halogen Metasomatism

The first step in evaluating the potential in situ origin of sodalite is to review previous work on feldspathoids in other groups of carbonaceous chondrites. Sodalite and nepheline occur in CAIs, chondrules, ameboid olivine aggregates, dark inclusions, and the matrix of the Allende-like oxidized subgroup of CV3 meteorites (CV_{OxA}; e.g., Krot et al. 1995). Feldspathoids are also present in the reduced subgroup of CVs (CV_{RED}), CO carbonaceous chondrites, and unequilibrated ordinary chondrites (Rubin 1998; Russell et al. 1998; Brearley and Krot 2013). With regard to the CV_{OxA} meteorites, feldspathoids and genetically related anhydrous minerals are interpreted to have formed by the metasomatic replacement of Ca-aluminosilicates, including melilite and anorthite in CAIs, and plagioclase feldspar and mesostasis glass in chondrules (MacPherson and Grossman 1984; McGuire and Hashimoto 1989; Brearley and Krot 2013).

The restriction of sodalite to the interior of MT75-1 suggests that a property of this CAI served to localize its crystallization, and by analogy the CVs, the presence of anorthite or melilite is the most likely reason. Replacement of anorthite ($CaAl_2Si_2O_8$) or gehlenite ($Ca_2Al[AlSi]O_7$) by sodalite would have required the import of Na and Cl and export of Ca (i.e., alkali-halogen metasomatism). This reaction could have taken place before or after aqueous alteration of MT75-1. A prehydration timing is preferred because melilite is highly reactive during aqueous alteration and has survived only in the most pristine CMs, namely Murchison (CM2.5; Armstrong et al. 1982), Paris (CM2.7; Hewins et al. 2014; Marrocchi et al. 2014), EET 96029 (CM2.7; Lee et al. 2016), and Jbilet Winselwan (CM2.7–2.4; King et al. 2018). MET 01075 by contrast is classified as CM2.2 and so has been much more highly altered. The presence of tochilinite-rich TCI particles in the matrix of MET 01075 is also evidence against significant posthydration heating that would have accompanied late-stage metasomatism. We therefore conclude that sodalite replaced melilite (or anorthite) during early alkali-halogen metasomatism at >~100 °C, after which the CAI and host meteorite underwent lower temperature (<~80 °C) aqueous alteration to form serpentine, tochilinite, and calcite (Fig. 6). This sequence of events requires sodalite to have survived parent body aqueous alteration. While its juxtaposition with phyllosilicate (Fig. 5) demonstrates that it did come into contact with liquid water, we argue that the relatively large size of the CAI inhibited ingress of aqueous solutions thus helping to preserve some of the sodaite.

The mineralogy of MET 01075 shows that it has sampled a parent body region that has undergone two phases of fluid/rock interaction, namely alkali-halogen metasomatism followed by aqueous alteration. This finding is difficult to reconcile with a model whereby parent body aqueous alteration is driven solely by the melting of accreted ices in response to radiogenic heating (Grimm and McSween 1989; Cohen and Coker 2000). Assuming static aqueous fluids (Bland et al. 2009), successive generations of alteration products that had formed under such conditions should record temperatures that were stable, or increased over time (i.e., a prograde reaction path) depending on how quickly they formed relative to the rate of heating. However, the formation of sodalite before serpentine and tochilinite indicates that temperatures fell overall. This discrepancy between predictions of the radiogenic heating model and our inferred evolution of MET 01075 can be explained by two models. In model 1, sodalite-forming metasomatism was driven by an early and short-lived heating event due to an impact that also formed the foliation petrofabric. Impedance of low intensity impacts (e.g., 1.5 km s^{-1}) through pore collapse could have generated temperature excursions within the fine-grained matrix that were more than sufficient to melt accreted ices (Bland et al. 2014). Model 1 requires that aqueous alteration took place subsequently as the system reverted to the radiogenic heating path (Fig. 6). In model 2, metasomatism was driven by unusually high temperature radiogenic heating, which subsequently passed into aqueous alteration. The petrofabric-forming impact was a late-stage event and also responsible for mixing of aqueously altered lithologies (i.e., incorporation of the clast; Fig. 6).

Implications for Understanding CM Parent Body History

Regardless of whether alkali-halogen metasomatism was initiated by an impact or radiogenic heating, it

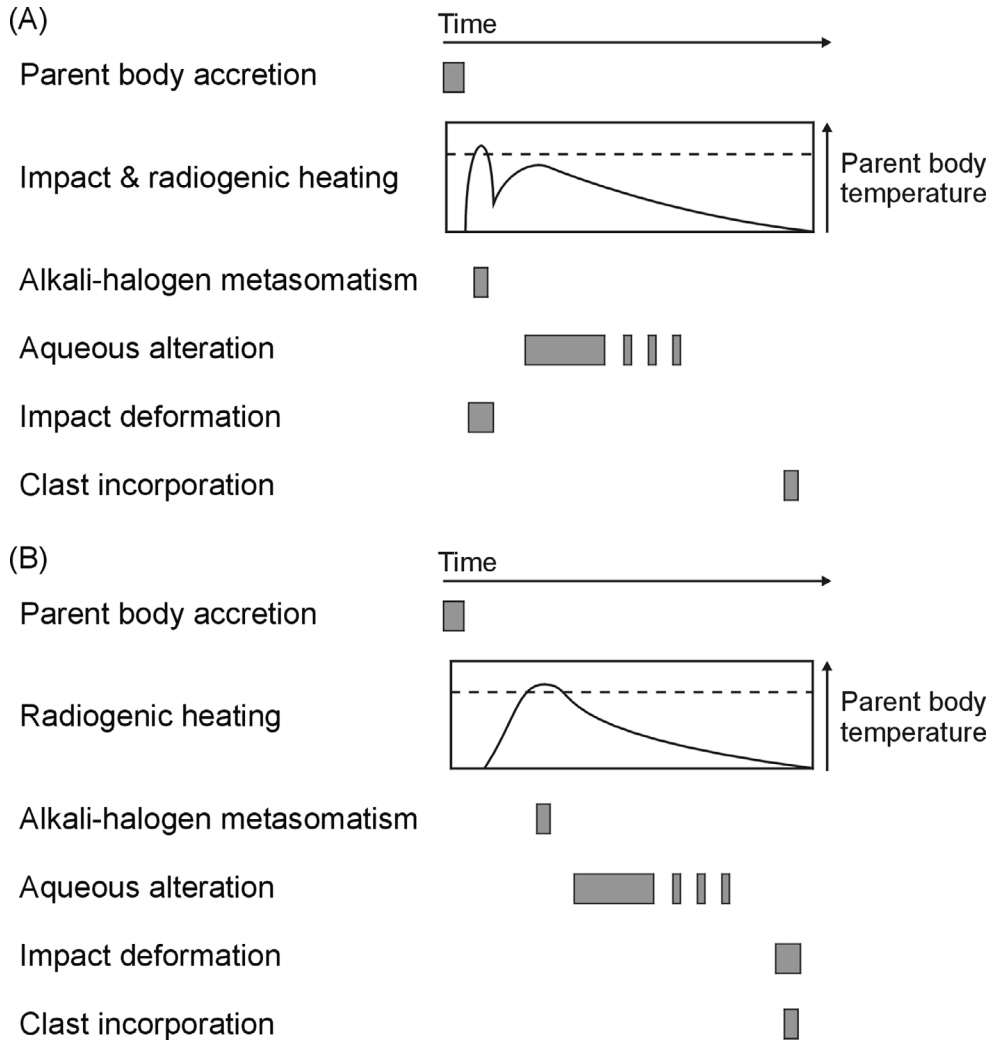

Fig. 6. The two models for in situ metasomatism. The qualitative thermal profiles are based on models in Fujiya et al. (2012), and dashed lines denote the temperature threshold for metasomatism. A) Model 1, whereby metasomatism is triggered by an early impact and later aqueous alteration is driven by radiogenic heating. Clast incorporation is a separate and later event. B) Model 2, whereby metasomatism is solely from radiogenic heating. The petrofabric forms by a late-stage and posthydration impact that was also responsible for incorporation of the clast. The lack of evidence for dehydroxylation of the phyllosilicates shows that such a late-stage impact would not have significantly heated the parent body region sampled by MET 01075.

could have been a widespread process in the CM parent body(ies) but with the evidence being almost completely erased by later aqueous alteration. Possible support for this idea comes from the Paris CM carbonaceous chondrite. Hewins et al. (2014) described an 800 μm size CAI (2010-05-01) in Paris that contains spinel, perovskite, gehlenite, anorthite, grossite, forsterite, diopside, kamacite, hibonite, and serpentine. This CAI is also host to a mineral that has partially replaced melilite and was described as a "silicate rich in O, Al, and Na, i.e., with a zeolite-like composition, and with minor S and Cl" (Hewins et al. 2014). The chemical composition of this mineral and its petrographic context (i.e., replacing melilite) suggests that it is sodalite. We speculate that sodalite has been preserved in Paris because this meteorite was only mildly aqueously altered after metasomatism. The lack of evidence for impact compaction of Paris favors the radiogenic heating model for alkali-halogen metasomatism of both these meteorite and MET 01075. The identity of the Al, Na, O, S, Cl bearing silicate (e.g., sodalite or zeolite) should be confirmed by future work on Paris.

CONCLUSIONS

MET 01075 sodalite provides a glimpse of an early phase of high temperature water–rock interaction within

the CM parent body(ies). Our principal findings are as follows:

1. MET 01075 is a relatively highly aqueously altered CM carbonaceous chondrite that is distinctive in having an impact-formed foliation petrofabric, and a matrix composed mainly of TCI particles.
2. Sodalite occurs within a single large CAI.
3. The sodalite could have formed by metasomatism of the CAI in a precursor body prior to its incorporation into the MET 01075 parent body. However, good physical preservation of the CAI argues against the excavation and reaccretion required by this scenario. Although formation of sodalite by interaction of the CAI with a nebular gas is also conceivable, evidence from the CV chondrites indicates that this mechanism is highly unlikely.
4. Our preferred model is that the sodalite replaced melilite or anorthite during in situ alkali-halogen metasomatism. Feldspathoid formation was followed by aqueous alteration of the matrix, chondrules/chondrule fragments, and the CAI. This later phase of lower temperature water–rock interaction may have destroyed products of alkali-halogen metasomatism elsewhere in the meteorite.
5. The driver of metasomatism could have been heating accompanying an early impact, which may also have generated the petrofabric. Alternatively, sodalite might have formed during radiogenic heating, with metasomatism passing into aqueous alteration as the system cooled. In this second scenario, impact compaction would have been a late-stage event and coincident with incorporation of the clast.
6. Our model for in situ alkali-halogen metasomatism should be tested by the analysis of other CM carbonaceous chondrites, particularly those that have been mildly aqueously altered (e.g., Paris) and so are most likely to preserve early formed feldspathoids.

Acknowledgments—We thank John Gilleece (University of Glasgow) for preparing the polished block, Peter Chung (University of Glasgow) for help with the SEM work, and Chris Hayward (University of Edinburgh) for assistance with the EMPA. We are grateful to ANSMET for providing the sample of MET 01075,8. U.S. Antarctic meteorite samples are recovered by the Antarctic Search for meteorites (ANSMET) program which has been funded by NSF and NASA, and characterized and curated by the Department of Mineral Sciences of the Smithsonian Institution and Astromaterials Acquisition and Curation Office at NASA Johnson Space Center. This work was funded by the Science and Technology Facilities Council through grants ST/N000846/1, ST/K000942/1, and ST/R000727/1. We thank Sasha Krot, Kazushige Tomeoka, and Adrian Brearley for very helpful reviews.

AUTHOR CONTRIBUTIONS

M.R.L. designed the research project; M.R.L., B.E.C., and A.J.K. undertook analyses and contributed to writing and editing of the paper; M.R.L. and A.J.K. acquired funding.

Editorial Handling—Dr. Adrian Brearley

REFERENCES

Akai J. 1988. Incompletely transformed serpentine-type phyllosilicates in the matrix of Antarctic CM chondrites. *Geochimica et Cosmochimica Acta* 52:1593–1599.

Akai J. 1992. T-T–T diagram of serpentine and saponite, and estimation of metamorphic degree of Antarctic carbonaceous chondrites. *Proceedings NIPR Symposium Antarctic Meteorites* 5:120–135.

Alexander C. M. O'D., Bowden R., Fogel M. L., Howard K. T., Herd C. D. K., and Nittler L. R. 2012. The provenances of asteroids, and their contributions to the volatile inventories of the terrestrial planets. *Science* 337:721–723.

Alexander C. M. O'D., Howard K. T., Bowden R., and Fogel M. L. 2013. The classification of CM and CR chondrites using bulk H, C and N abundances and isotopic compositions. *Geochimica et Cosmochimica Acta* 123:244–260.

Alexander C. M. O'D., Bowden R., Fogel M. L., and Howard K. T. 2015. Carbonate abundances and isotopic compositions in chondrites. *Meteoritics & Planetary Science* 50:810–833.

Armstrong J. T., Meeker G. P., Huneke J. C., and Wasserburg G. J. 1982. The Blue Angel: I. The mineralogy and petrogenesis of a hibonite inclusion from the Murchison meteorite. *Geochimica et Cosmochimica Acta* 46:575–595.

Baker L., Franchi I. A., Wright I. P., and Pillinger C. T. 2002. The oxygen isotopic composition of water from Tagish Lake: Its relationship to low-temperature phases and to other carbonaceous chondrites. *Meteoritics & Planetary Science* 37:977–985.

Barber D. J. 1981. Matrix phyllosilicates and associated minerals in C2M carbonaceous chondrites. *Geochimica et Cosmochimica Acta* 45:945–970.

Bischoff A., Scott E. R. D., Metzler K., and Goodrich C. A. 2006. Nature and origins of meteoritic breccias. In *Meteorites and the early solar system II*, edited by Lauretta D. S. and McSween H. Y. Jr. Tucson, AZ: The University of Arizona Press. pp. 679–712.

Bland P. A., Jackson M. D., Coker R. F., Cohen B. A., Webber J. B. W., Lee M. R., Duffy C. M., Chater R. J., Ardakani M. G., McPhail D. S., McComb D. W., and Benedix G. K. 2009. Why aqueous alteration in asteroids was isochemical: High porosity≠high permeability. *Earth and Planetary Science Letters* 287:559–568.

Bland P. A., Collins G. S., Davison T. M., Abreu N. M., Ciesla F. J., Muxworthy A. R., and Moore J. 2014. Pressure–temperature evolution of primordial solar system

solids during impact-induced compaction. *Nature Communications* 5:5451.

Brearley A. J., and Krot A. N. 2013. Metasomatism in the early solar system: The record from chondritic meteorites. In *Metasomatism and the chemical transformation of rock*. Lecture notes in Earth system sciences. Berlin: Springer.

Bunch T. E. and Chang S. 1980. Carbonaceous chondrites—II. Carbonaceous chondrite phyllosilicates and light element geochemistry as indicators of parent body processes and surface conditions. *Geochimica et Cosmochimica Acta* 44:1543–1577.

Cohen B. A. and Coker R. A. 2000. Modeling of liquid water on CM meteorite parent bodies and implications for amino acid racemization. *Icarus* 145:369–381.

Cressey G. and Schofield P. F. 1996. Rapid whole-pattern profile stripping method for the quantification of multiphase samples. *Powder Diffraction* 11:35–39.

Fujiya W., Sugiura N., Hotta H., Ichimura K., and Sano Y. 2012. Evidence for the late formation of hydrous asteroids from young meteoritic carbonates. *Nature Communications* 3:627.

Greenwood R. C., Lee M. R., Hutchison R., and Barber D. J. 1994. Formation and alteration of CAIs in Cold Bokkeveld (CM2). *Geochimica et Cosmochimica Acta* 58:1913–1935.

Grimm R. E. and McSween H. Y. Jr. 1989. Water and the thermal evolution of carbonaceous chondrite parent bodies. *Icarus* 82:244–280.

Guo W. and Eiler J. M. 2007. Temperatures of aqueous alteration and evidence for methane generation on the parent bodies of the CM chondrites. *Geochimica et Cosmochimica Acta* 71:5565–5575.

Hanna R. D., Ketcham R. A., Zolensky M., and Behr W. M. 2015. Impact-induced brittle deformation, porosity loss, and aqueous alteration in the Murchison CM chondrite. *Geochimica et Cosmochimica Acta* 171:256–282.

Hewins R. H., Bourot-Denise M., Zanda B., Leroux H., Barrat J.-A., Humayun M., Göpel C., Greenwood R. C., Franchi I. A., Pont S., Lorand J.-P., Cournède C., Gattacceca J., Rochette P., Kuga M., Marrocchi Y., and Marty B. 2014. The Paris meteorite, the least altered CM chondrite so far. *Geochimica et Cosmochimica Acta* 124:190–222.

Howard K. T., Alexander C. M. O'D., Schrader D. L., and Dyl K. A. 2015. Classification of hydrous meteorites (CR, CM and C2 ungrouped) by phyllosilicate fraction: PSD-XRD modal mineralogy and planetesimal environments. *Geochimica et Cosmochimica Acta* 149:206–222.

Ikeda Y. and Kimura M. 1995. Anhydrous alteration of Allende chondrules in the solar nebula I: Description and alteration of chondrules with known oxygen-isotopic compositions. *Proceedings NIPR Symposium Antarctic Meteorites* 8:97–122.

Ikeda Y. and Kimura M. 1996. Anhydrous alteration of Allende chondrules in the solar nebula III: Alkali-zoned chondrules and heating experiments for anhydrous alteration. *Proceedings NIPR Symposium Antarctic Meteorites* 9:51–68.

King A. J., Schofield P. F., Howard K. T., and Russell S. S. 2015. Modal mineralogy of CI and CI-like chondrites by X-ray diffraction. *Geochimica et Cosmochimica Acta* 165:148–160.

King A. J., Schofield P. F., and Russell S. S. 2017. Type 1 aqueous alteration in CM carbonaceous chondrites: Implications for the evolution of water-rich asteroids. *Meteoritics & Planetary Science* 52:1197–1215.

King A. J., Russell S. S., Schofield P. F., Humphreys-Williams E. R., Strekopytov S., Abernathy F. A. J., Verchovsky A. B., and Grady M. M. 2018. The alteration history of the Jbilet Winselwan CM carbonaceous chondrite: An analog for C-type asteroid sample return. *Meteoritics & Planetary Science* 54:521–543.

Krot A. N., Scott E. R. D., and Zolensky M. E. 1995. Mineralogical and chemical modification of components in CV3 chondrites: Nebular or asteroidal processing? *Meteoritics* 30:748–776.

Krot A. N., Petaev M. I., Zolensky M. E., Keil K., Scott E. R. D., and Nakamura K. 1998a. Secondary calcium-iron-rich minerals in the Bali-like and Allende-like oxidized CV3 chondrites and Allende dark inclusions. *Meteoritics & Planetary Science* 33:623–645.

Krot A. N., Petaev M. I., Scott E. R. D., Choi B.-G., Zolensky M. E., and Keil K. 1998b. Progressive alteration in CV3 chondrites: More evidence for asteroidal alteration. *Meteoritics & Planetary Science* 33:1065–1085.

Lee M. R. 1993. The petrography, mineralogy and origins of calcium sulphate within the Cold Bokkeveld CM carbonaceous chondrite. *Meteoritics* 28:53–62.

Lee M. R., Bland P. A., and Graham G. 2003. Preparation of TEM samples by focused ion beam (FIB) techniques: Applications to the study of clays and phyllosilicates in meteorites. *Mineralogical Magazine* 67:581–592.

Lee M. R., Lindgren P., Sofe M. R., Alexander C. M. O'D., and Wang J. 2012. Extended chronologies of aqueous alteration in the CM2 carbonaceous chondrites: Evidence from Queen Alexandra Range 93005. *Geochmica et Cosmochimica Acta* 92:148–169.

Lee M. R., Lindgren P., King A. J., Greenwood R. C., Franchi I. A., and Sparkes R. 2016. Elephant Moraine 96029, a very mildly aqueously altered and heated CM carbonaceous chondrite: Implications for the drivers of parent body processing. *Geochimica et Cosmochimica Acta* 187:237–259.

Lindgren P., Hanna R. D., Dobson K. J., Tomkinson T., and Lee M. R. 2015. The paradox between low shock-stage and evidence for compaction in CM carbonaceous chondrites explained by multiple low-intensity impacts. *Geochimica et Cosmochimica Acta* 148:159–178.

MacPherson G. J. and Grossman L. 1984. "Fluffy" type A Ca, Al-rich inclusions in the Allende meteorite. *Geochimica et Cosmochimica Acta* 48:29–46.

Marrocchi Y., Gounelle M., Blanchard I., Caste F., and Kearsley A. T. 2014. The Paris meteorite: secondary minerals and asteroidal processing. *Meteoritics & Planetary Science* 49:1232–1249.

McGuire A. V. and Hashimoto A. 1989. Origin of zoned fine-grained inclusions in the Allende meteorite. *Geochimica et Cosmochimica Acta* 53:1123–1133.

McSween H. Y. Jr. 1979a. Are carbonaceous chondrites primitive or processed? A review. *Reviews in Geophysics and Space Physics* 17:1059–1078.

McSween H. Y. Jr. 1979b. Alteration in CM carbonaceous chondrites inferred from modal and chemical variations in matrix. *Geochimica et Cosmochimica Acta* 43:1761–1770.

Metzler K., Bischoff A., and Stöffler D. 1992. Accretionary dust mantles in CM chondrites: Evidence for solar nebula processes. *Geochimica et Cosmochimica Acta* 56:2873–2897.

Nakamura T. 2006. Yamato 793321 CM chondrite: Dehydrated regolith material of a hydrous asteroid. *Earth and Planetary Science Letters* 242:26–38.

Palme H. and Warke D. A. 1988. CV-chondrites: High temperature gas solid equilibrium vs. parent body metamorphism. Proceedings, 19th Lunar and Planetary Science Conference. pp. 897–898.

Rubin A. E. 1998. Correlated petrologic and geochemical characteristics of CO3 chondrites. *Meteoritics & Planetary Science* 33:383–391.

Rubin A. E. 2012. Collisional facilitation of aqueous alteration of CM and CV carbonaceous chondrites. *Geochimica et Cosmochimica Acta* 90:181–194.

Rubin A. E., Trigo-Rodrigues J. M., Huber H., and Wasson J. T. 2007. Progressive aqueous alteration of CM carbonaceous chondrites. *Geochimica et Cosmochimica Acta* 71:2361–2382.

Russell S. S., Huss G. R., Fahey A. J., Greenwood R. C., Hutchison R., and Wasserburg G. J. 1998. An isotopic and petrologic study of calcium-aluminium-rich inclusions from CO3 meteorites. *Geochimica et Cosmochimica Acta* 62:689–714.

Russell S. S., Zipfel J., Folco L., Jones R., Grady M. M., McCoy T., and Grossman J. N. 2003. The Meteoritical Bulletin, No. 87. *Meteoritics & Planetary Science* 38:A189–A248.

Scott E. R. D., Keil K., and Stöffler D. 1992. Shock metamorphism of carbonaceous chondrites. *Geochimica et Cosmochimica Acta* 56:4281–4293.

Tonui E., Zolensky M., Hiroi T., Nakamura T., Lipschutz M. E., Wang M.-S., and Okudaira K. 2014. Petrographic, chemical and spectroscopic evidence for thermal metamorphism in carbonaceous chondrites I: CI and CM chondrites. *Geochimica et Cosmochimica Acta* 126:284–306.

Verdier-Paoletti M. J., Marrocchi Y., Avice G., Roskosz M., Gurenko A., and Gounelle M. 2017. Oxygen isotope constraints on the alteration temperatures of CM chondrites. *Earth and Planetary Science Letters* 458:273–281.

Zolensky M. E., Bourcier W. L., and Gooding J. L. 1989. Aqueous alteration on the hydrous asteroids: Results of EQ3/6 computer simulations. *Icarus* 78:411–425.

Zolensky M. E., Mittlefehldt D. W., Lipschutz M. E., Wang M.-S., Clayton R. N., Mayeda T. K., Grady M. M., Pillinger C., and Barber D. 1997. CM chondrites exhibit the complete petrologic range from type 2 to 1. *Geochimica et Cosmochimica Acta* 61:5099–5115.